RAA 2020 Vol. **20** No. **2**, 22(10pp) doi: 10.1088/1674–4527/20/2/22

http://www.raa-journal.org *http://iopscience.iop.org/raa*

Research in Astronomy and Astrophysics

Periodic variation and phase analysis of grouped solar flare with sunspot activity

Hui Deng[1,2], Ying Mei[1] and Feng Wang*[1,2,3]

[1] Center For Astrophysics, Guangzhou University, Guangzhou 510006, China; *fengwang@gzhu.edu.cn*
[2] CAS Key Laboratory of Solar Activity, National Astronomical Observatories, Chinese Academy of Sciences, Beijing 100101, China
[3] Kunming University of Science and Technology, Kunming 650051, China

Received 2019 July 12; accepted 2019 July 31

Abstract Studies on the periodic variation and the phase relationship between different solar activity indicators are useful for understanding the long-term evolution of solar activity cycles. Here we report the statistical analysis of grouped solar flare (GSF) and sunspot number (SN) during the time interval from January 1965 to March 2009. We find that, (1) the significant periodicities of both GSF and SN are related to the differential rotation periodicity, the quasi-biennial oscillation (QBO), and the eleven-year Schwabe cycle (ESC), but the specific values are not absolutely identical; (2) the ESC signal of GSF lags behind that of SN with an average of 7.8 months during the considered time interval, which implies that the systematic phase delays between GSF and SN originate from the inter-solar-cycle signal. Our results may provide evidence about the storage of magnetic energy in the corona.

Key words: Sun: sunspots — Sun: flares — Sun: activity — Sun: magnetic fields

1 INTRODUCTION

Understanding the dynamic processes of the solar interior and atmosphere, and how they produce the long-term cyclic variation continues to challenge the solar communities (Cameron et al. 2017). The available solar databases provide a broader chance, showing a wide variety of periodic behavior, phase asynchrony, hemispheric coupling, chaotic behavior, fractal property as well as cycle amplitude and length (Deng et al. 2016a,b). Furthermore, advances in data analysis techniques, such as time-frequency analysis and machine deep learning, are now inspiring studies that allow us to further explore the nonlinear dynamics of the Sun in far greater detail (Deng et al. 2012).

During the past few decades, the statistical relationship between solar flare activity and sunspot number (or sunspot area) has attracted interest. Wagner (1988) reported that solar flare occurrence and background flux in the soft X-ray (SXR) wavelength are delayed with respect to sunspot activity, and the relative phase shifts are around two to three years between the peak times during solar cycle 21. Because the SXR flare occurrence and background flux are considered to be dominated by the post-flares emission from the dominant active regions, so Aschwanden (1994) interpreted that the phase delay is possibly due to the increasing complexity of coronal magnetic structures in the decay phase of the solar cycle. By studying the temporal variation of SXR background flux and its relation to the flaring rate, energetic event rate, and the solar cycle, Wilson (1993) did not find any evidence for the phase delay between SXR flare occurrence and sunspot activity during solar cycle 22 (from January 1986 to May 1992). If the solar cycles 21 and 22 are considered together, then the average phase delay derived from the correlation analysis is found to be 6 months, as studied by Wheatland & Litvinenko (2001).

To describe how the magnetic free energy in the solar corona varies in response to variations in the supply of energy to the system and to changes in the flaring rate, Wheatland & Litvinenko (2001) presented a detailed model for dynamic energy balance in the corona over the solar cycle. Their model predicted that both the flaring rate and the free energy of the system lag behind the driving of the system with a lag of around 11 months. To test the results of their model, Temmer et al. (2003) analyzed the temporal evolution of solar flare occurrence with respect to sunspot activity during solar cycles 19–23. They

* Corresponding author

found that, for solar cycles 19, 21 and 23 (namely, odd solar cycles), a characteristic phase lag between flare activity and sunspot activity is in the range from 10 to 15 months, which is consistent with the model predictions by Wheatland & Litvinenko (2001). However, no characteristic phase lag larger than zero is found for solar cycles 20 and 22 (namely, even solar cycles). Feng et al. (2013) studied the phase relationship between grouped solar flare and sunspot number by several time-frequency analysis methods, they found that the phase relationship between the two is not only time-dependent but also frequency-dependent, which implies that their relationship is a complex nonlinear relationship. The relationships between solar flare parameters (such as the total importance, the time duration, the flare index, and the flux) and sunspot activity as well as those between geomagnetic activity (aa index) and the flare parameters was well studied by Du & Wang (2012), they found that their relationship can be well described by an integral response model with the response time scales of about 8 and 13 months, respectively. In other words, solar flare is considered to be related to the accumulation of solar magnetic energy in the past through a time decay factor, and it will help the researchers to understand the mechanism of solar flares and to improve the prediction of the solar flares. Du (2011) proposed an integral response model to describe the relationship between geomagnetic activity and solar activity (represented by sunspot number, and the proposed model can naturally explain some phenomena related to geomagnetic activity and solar activity, such as the phase lag between flare activity and sunspot number.

The periodic scales of solar activity indices have a broad range, varying from several days to tens of years. Except for the 27-day rotation period and the 11-year Schwabe cycle, many other quasi-periodicities are found in the past seven decades. For example, Kilcik et al. (2010) studied the periodicities of solar flare index during solar cycles 21–23, and found that a lesser number of periodicities is found in the range of low frequencies (long periods) while the higher frequencies display a great number of periodicities. They also found that the periodicities of solar activity in different solar cycles are not identical. For the temporal features between solar flare activity and sunspot number or area, the clear relationships are not fully studied. For instance, we do not know whether the periodicities of flare occurrence and sunspot activity are identical, and whether the phase relationship between flare activity and sunspot activity depends on the considered periodicities. Therefore, it is necessary to study the quasi-periodic variations and the phase relationship between solar flare occurrence and sunspot activity.

In this paper, we report the periodic variation and phase relationship between grouped solar flare and sunspot numbers during the time interval from January 1965 to March 2009 (solar cycles 20–23). Two nonlinear time-frequency analysis techniques are applied in this work, namely the ensemble empirical mode decomposition (EEMD) and the cross-recurrence plot (CRP). In Section 2, the data sets and the analysis methods are introduced. The statistical analysis results are shown in Section 3. Finally, the main conclusions are summarized in Section 4.

2 DATA SETS AND ANALYSIS METHODS

2.1 Observational Time Series

The grouped solar flare (GSF) time series is publicly downloaded from the website of the National Geophysical Data Center (NGDC)[1]. The time interval of GSF data set is from January 1965 to March 2009, almost covering solar cycles 20–23. The term "grouped" means the observations of the same flare event by different solar sites were lumped together and counted as one. This indicator is thus different from the classical flare activity indices, such as Hα flare index, soft X-ray flare, and hard X-ray flare (Gupta et al. 2007).

The sunspot number (SN) data set is freely obtained from the World Data Center (WDC) — Sunspot Index and Long-term Solar Observations (SILSO), Royal Observatory of Belgium, Brussels[2]. The SN time series (version 2.0) begins from January 1749 to April 2019 and is updated every month (Clette et al. 2014). Here, the time period from January 1965 to March 2009, the common time interval to the GSF data, is extracted.

Figure 1 displays the monthly counts of GSF (upper panel) and SN (lower panel) during the time period from January 1965 to March 2009, covering the solar cycles 20–23. As the figure shows, the temporal evolution of GSF obviously differs from that of SN, indicating that they exhibit different features.

2.2 Methods of Analysis

2.2.1 Ensemble empirical mode decomposition

Contrary to the traditional data decomposing techniques, the empirical mode decomposition (EMD) is an empirical, intuitive, and adaptive method, without requiring any predetermined basis functions. This time-frequency analysis method was first proposed by Huang et al. (1998) and has been applied in many research fields. For solar physics

[1] `ftp://ftp.ngdc.noaa.gov/STP/SGD/sgdpdf/Number_of_Solar_Flares.pdf`

[2] `http://www.sidc.be/silso/datafiles`

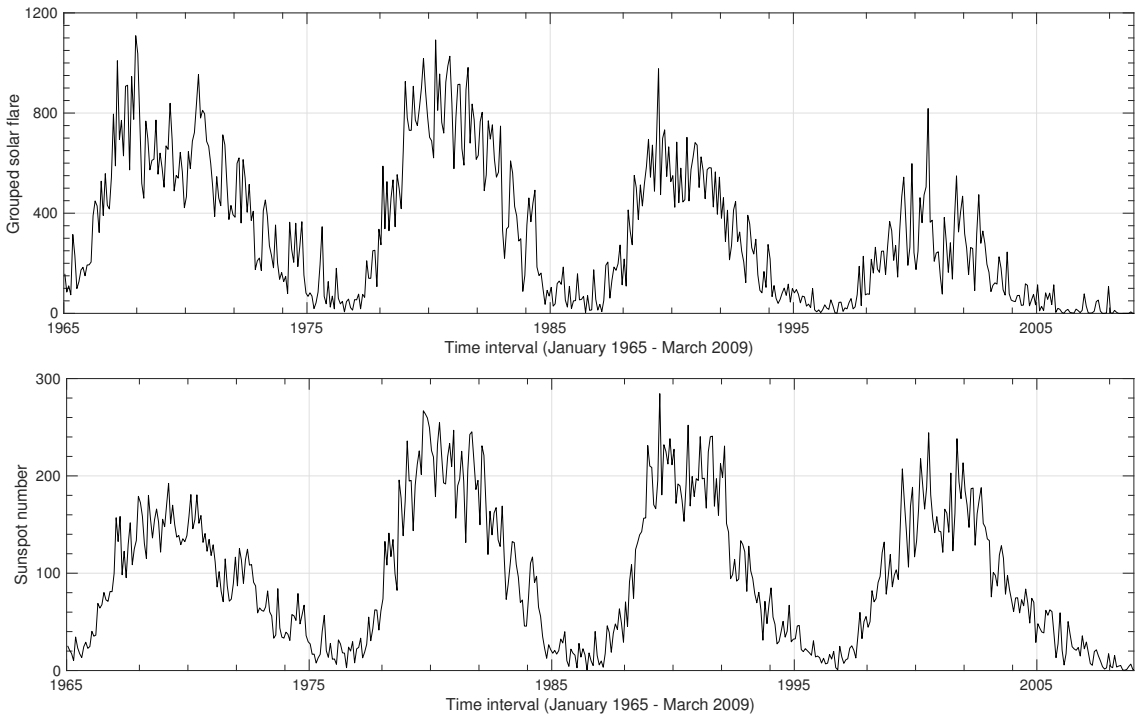

Fig. 1 Monthly counts of grouped solar flare (*upper panel*) and sunspot number (*lower panel*) during the time interval from January 1965 to March 2009.

studies, Li et al. (2012a) applied it to decompose the solar constant into three components: the rotation signal, the annual-variation, and the inter-solar-cycle signal; to study the periodic components of polar faculae and coronal green line intensity, Deng et al. (2014) and Deng et al. (2015) used the EMD to reveal the long-term temporal variation of solar time series; Xiang & Qu (2016) used it to extract the intrinsic mode functions (IMFs) of the solar mean magnetic field observed at the Wilcox Solar Observatory, and they then studied the relation of these IMFs with other solar activity indicators.

The EMD is usually applied to decompose a signal $x(t)$ into a series of mono-component contributions designated as IMF and a secular trend (or a constant), namely:

$$x(t) = \sum_{i=1}^{n} s_i(t) + r_n \,, \tag{1}$$

where r_n is the residue (either a trend or a constant) after the n IMFs are extracted. Generally speaking, the first IMF s_1 contains the shortest periodic scale of the original signal. For an IMF, it should satisfy two conditions: (1) in the whole data set, the number of extrema and the number of zero crossings must either equal or differ at most by one; and (2) at any point, the mean value of the upper envelope and lower envelope is zero (Deng et al. 2013a; Qu et al. 2015; Gao 2017).

The major drawbacks of the EMD is the frequent appearance of mode mixing, which is defined as a single IMF either consisting of signals of widely disparate scales or a signal of a similar scale residing in different IMFs. To deal with the mode mixing problem, a noise-assisted data analysis method called the ensemble EMD (EEMD) is proposed by Wu & Huang (2011). The EEMD, which defines the true IMFs as the mean of an ensemble of trials, each consisting of the signal plus a white noise of finite amplitude. This technique is based on the insight gleaned from statistical studies of the inherent properties of white noise, which indicated that it is inspired by the noise-added analysis initiated by Wu & Huang (2004). In our analysis, this powerful approach is applied to decompose the solar time series.

2.2.2 *Cross-recurrence plot*

In the last three decades, the technique of recurrence plot (RP) has been considered as a method to describe the complex dynamics of the nonlinear and non-stationary systems (Eckmann et al. 1987). An RP is a representation of recurrent states of a dynamical system in its m-dimensional phase space (Marwan et al. 2007). From a mathematic point of view, it is a pairwise test of all phase space vectors $\boldsymbol{x}_i \, (i = 1, \ldots, N, \boldsymbol{x} \in \mathcal{R}^m)$ among each other, whether or not they are close:

$$R_{i,j} = \Theta \left(\varepsilon - d \left(\boldsymbol{x}_i, \boldsymbol{x}_j \right) \right) \,, \tag{2}$$

where $\Theta(\cdot)$ is the Heaviside function, $\mathcal{E}$ is a threshold for proximity, and the closeness $d \left(\boldsymbol{x}_i, \boldsymbol{x}_j \right)$ could be measured

in different ways by using spatial distance or local rank order (Marwan et al. 2009).

To determine the dependencies between two different systems, the cross-recurrence plot (CRP) is introduced and can be considered as a bivariate extension of the RP (Zbilut et al. 1998). An important advantage of the CRP is that it could be used to reveal the local differences of the dynamical evolution of close trajectory segments, represented by bowed lines (Marwan & Kurths 2002). A time dilatation or time compression of trajectories leads to a distortion of the diagonal lines, showing the inner relationship between the slope of RP lines and local temporal transformations (Marwan et al. 2007). When the two systems are different, the main black diagonal will become somewhat disrupted and is named as line of synchronisation (LOS). Therefore, the LOS allows us to find the phase shift between two time series (Deng et al. 2017).

3 STATISTICAL ANALYSIS RESULTS

3.1 Periodic Variation of GSF and SN

For the EEMD method, the number of ensemble and the noise amplitude are the two parameters that are needed to be prescribed. As pointed out by Wu & Huang (2011), an ensemble number of a few hundred could bring out a good result, and the remaining noise would lead to only less than a fraction of 1% of error if the added noise has an amplitude that is a fraction of the standard deviation of the original time series. In our analysis, the number of ensemble is 100, and the added noise amplitude is 0.2 times of the standard deviation of the original data.

Because the EEMD method is a powerful algorithm to isolate signals with specific timescales in a given time series produced by different underlying physics (Li et al. 2012b; Gao et al. 2017), it is thus applied to extracted the IMFs of GSF and SN data sets. The decomposed results of GSF and SN, respectively, are shown in Figures 2 and 3. From these two figures, one can easily see that both data sets are decomposed into eight IMFs and a secular trend.

Obviously, the extracted IMFs of GSF and SN have time-dependent amplitudes and differ from pure sinusoidal functions. Actually, they are the intrinsic fluctuations decomposed directly from the time series using the shifting process and are pre-estimated functions. However, the IMFs capture the oscillations of the time series even though the data set is not-stationary and nonlinear. For example, the 11-year Schwabe cycle is clearly shown as the fifth extracted IMF in Figures 2 and 3.

Subsequently, to calculate the average periodicity and the uncertainty of each IMF for GSF and SN, the statistical significance test method proposed by Wu & Huang (2004) is applied. In this work, we selected two confidence-limit levels: 95% and 99%. Namely, the IMFs whose energy level lies above the spread lines, for the white noise, are statistically significant at 95 and 99 percent confidence levels. The uncertainty in the average periodicity is calculated from the standard errors ($\sigma/n^{1/2}$, where σ is the standard deviation and n is the number of data points).

Table 1 The average periodicities (in years) and the uncertainties of IMFs, which are extracted from GSF and SN, respectively.

	grouped solar flare	sunspot number
1	0.2405±0.0032	0.2405±0.0035
2	0.5145±0.0148	0.5206±0.0169
3	0.9219±0.0300	1.0536±0.0219
4	2.5731±0.1775	3.1350±0.5624
5	10.069±0.4102	11.698±0.4169
6	14.865±0.6325	17.221±1.8170
7	39.477±5.3529	46.484±4.7843

Figure 4 displays that for both GSF and SN, IMF1, IMF4, IMF5, and IMF6 are statistically significant at the 99% confidence level, and the other IMFs are below the 95% confidence level. Here, the periodicities those are below the 95% confidence level are not discussed, we only analyzed IMF1, IMF4, IMF5, and IMF6. The average periodicities and the uncertainties of each IMF for GSF and SN are collected in Table 1. As shown in Figure 4 and Table 1, the periodicity (0.2405 year, about 87.7 days) of IMF1 for both data sets is inferred to be three multiple harmonics of 29 days, which is approximately the periodicity of the differential rotation periodicity of the Sun (Xiang et al. 2014). The average periodicity of IMF4 for each data set is related to the typical timescale between 1 and 4 years, one is 2.5731±0.1775 years, and the other one is 3.1350±0.5624 years, they could be considered as the solar quasi-biennial oscillation (QBO). The physical origin of solar QBO may be related to the dynamic processes in the solar tachocline, although it is not yet fully understood (Bazilevskaya et al. 2014). The IMF5 values of GSF and SN should be the most prominent periodicities: the 11-year solar activity cycle, the so-called eleven-year Schwabe cycle (ESC). The periods of IMF6 are 14.865 years for GSF and 17.221 years for SN, respectively, and they are about 1.5 times (1.5×11 years=16.5 years) as long as the 11-year Schwabe cycle. Therefore, the significant periodicities of GSF and SN, which are above the 99% confidence level, are connected with the differential rotation periodicity, the quasi-biennial oscillation, and the 11-year Schwabe cycle.

3.2 Phase Relationship between GSF and SN

Although the previous studies have shown that solar flare activity lags behind the sunspot number (or area) with several to tens of months, these studies did not consider the different periodic scales that are responsible for the phase

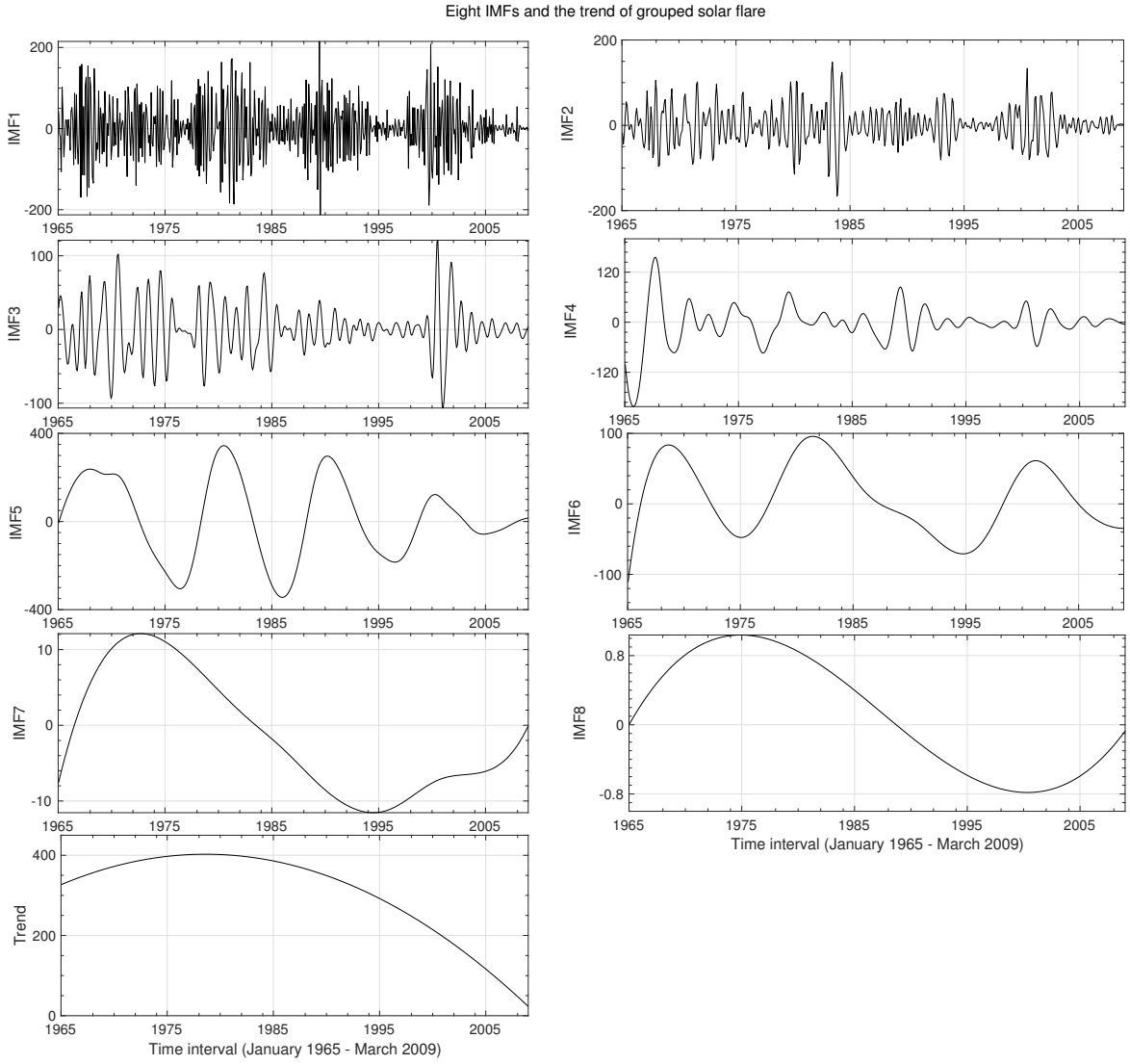

Fig. 2 The IMFs 1–8 and the trend of GSF generated by the EEMD method (with the ensemble size of 100).

difference. Here, two periodic scales are separately studied the phase relationship between GSF and SN, one is the QBO, and the other one is the ESC. To better understand their phase relationship, the cross-correlation analysis method is first used, and then the CRP technique is applied.

The upper panels of Figure 5 show the temporal variations of QBO (upper-left) and ESC (upper-right) signals of GSF and SN, respectively. From this figure one can see that their variabilities are not completely in phase, implying that they should be asynchronous in the given periodic scale. The lower panels of Figure 5 display the results of the cross-correlation analysis of QBO (lower-left) and ESC (lower-right) signals of GSF and SN with the phase shifts from –120 to 120 months. The abscissa implies the phase lag of GSF with respect to SN along the calendar-time axis, with the negative values representing the backward shifts. In our analysis, the phase lags are only considered between –120 and 120 months, so all of the local peaks are above the 95% confidence levels (shown by the dashed lines).

For the QBO signal, the correlation coefficient is 1 when there is no phase shift, implying that they are highly positive correlation. When the phase shifts are –87, –41, 41, and 87 months, the values of the correlation coefficient arrive at local maxima. The average interval between the two neighboring local maxima is 43.5±2.9 months (3.63±0.24 years). When the phase lags are –115, –67, −20, 20, 67, and 115 months, the values of the correlation coefficient reach local minima. The average interval between the two neighboring local minima is 46±3.4 months (3.83±0.28 years). For the ESC signal, the situation is very simple. Two signals are highly positive correlation, because the correlation coefficient is 1 when there is no phase shift. When the phase lags are –63 and 63 months,

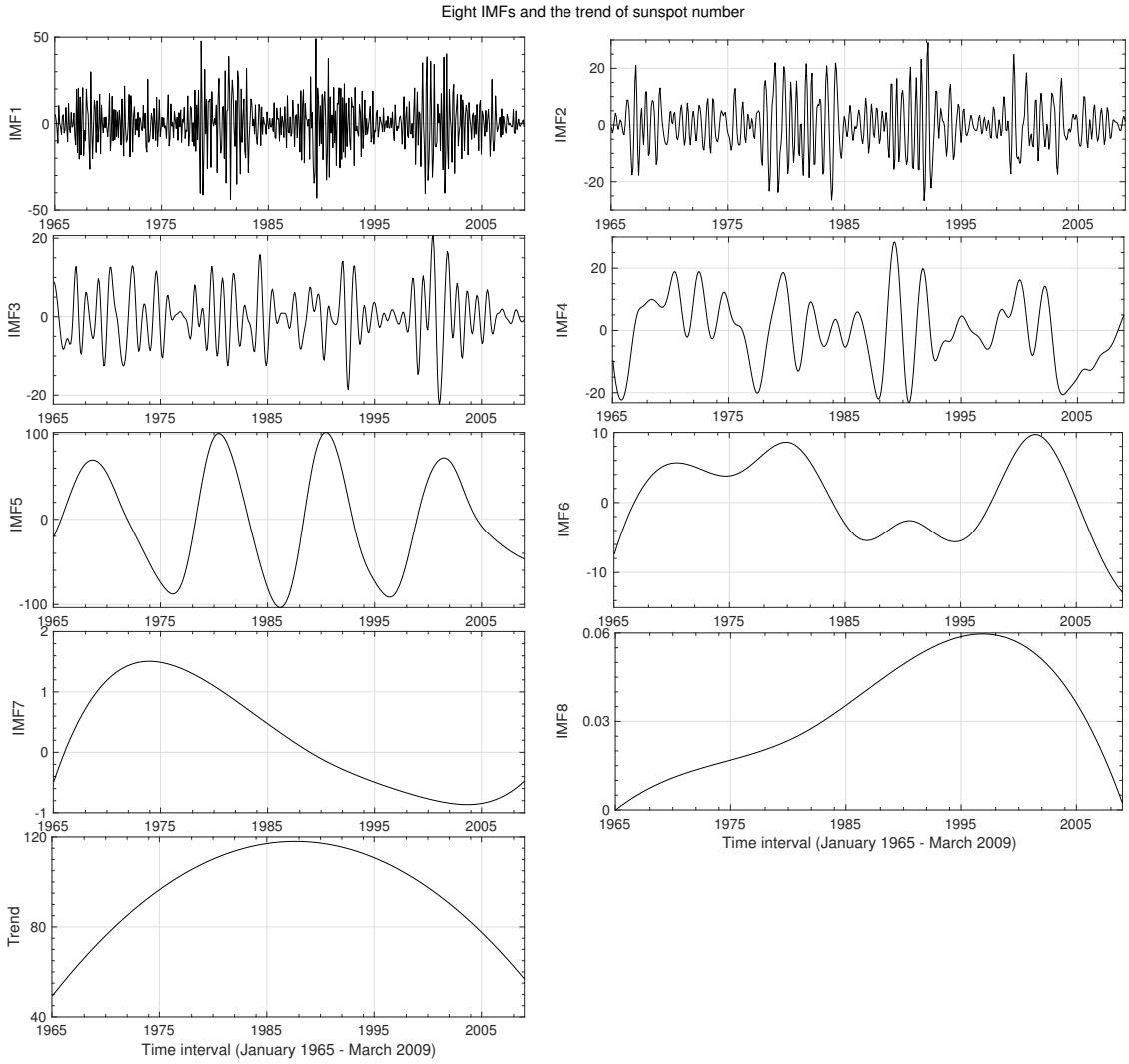

Fig. 3 The IMFs 1–8 and the trend of SN generated by the EEMD method (with the ensemble size of 100).

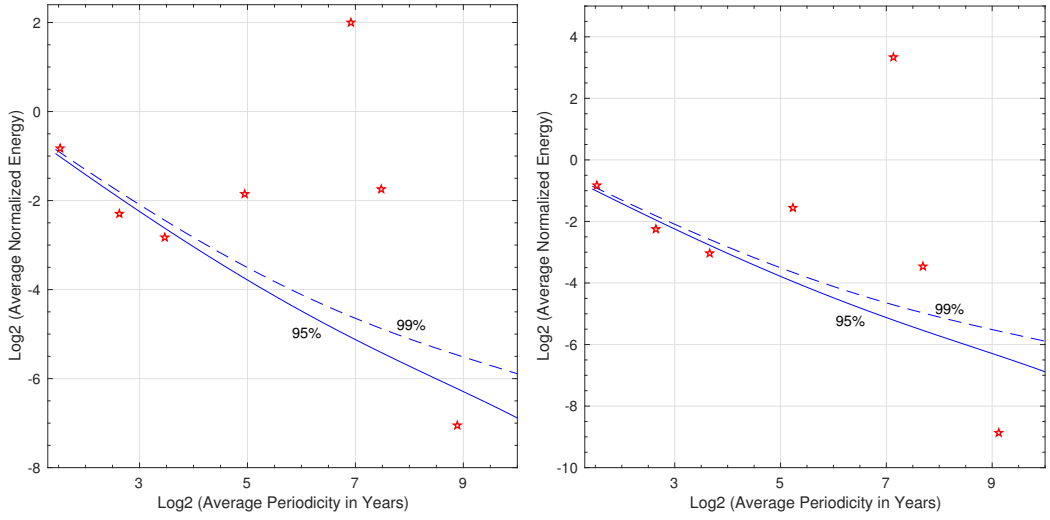

Fig. 4 Statistical significance test of seven IMFs of GSF (*left panel*) and SN (*right panel*) data sets, respectively. The *dashed* and the *solid lines* shown in each panel are the 99% and 95% confidence levels.

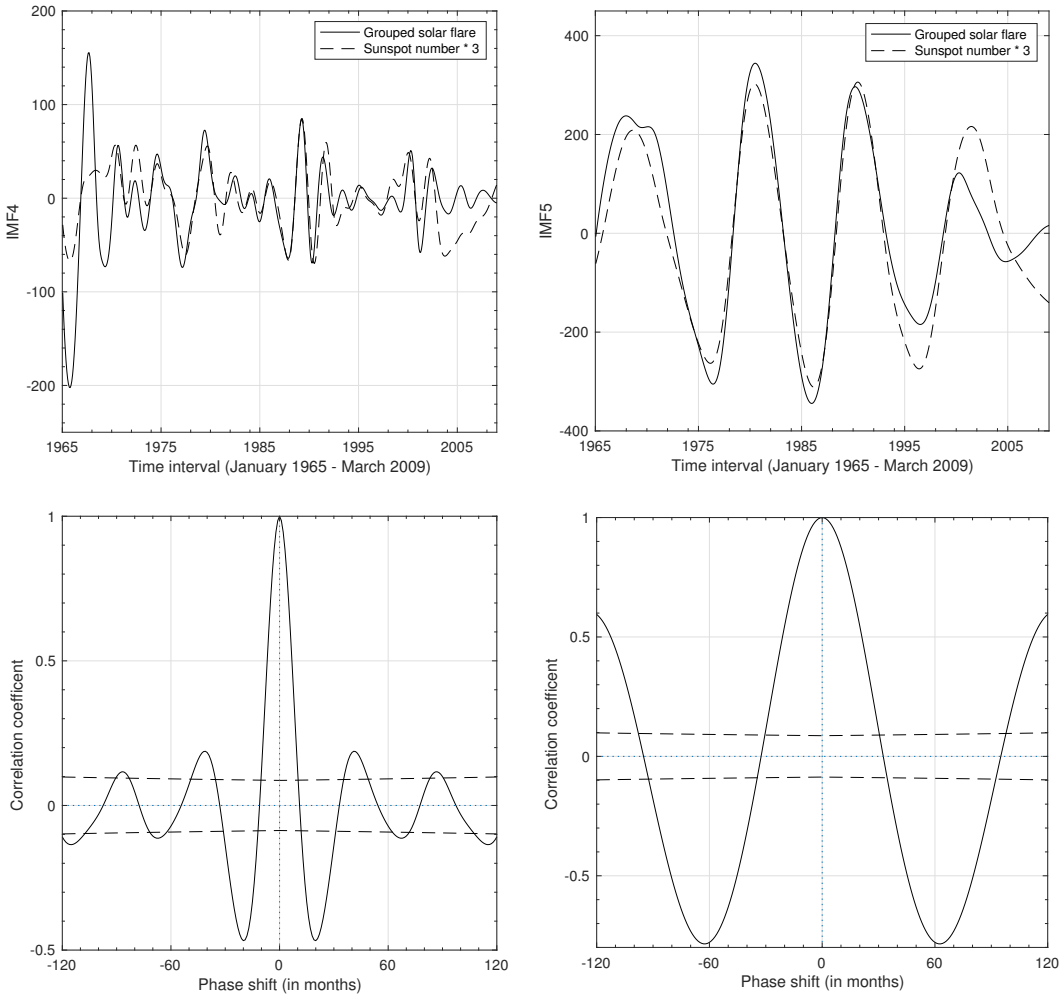

Fig. 5 *Upper-left panel*: temporal variation of QBO signal of GSF (*solid line*) and SN (*dashed line*). *Upper-right panel*: temporal variation of ESC signal of GSF (*solid line*) and SN (*dashed line*). *Lower-left panel*: the cross-correlation analysis results of the QBO signal between GSF and SN, and the *dashed lines* are the 95% confidence levels. *Lower-right panel*: the cross-correlation analysis results of the ESC signal between GSF and SN, and the *dashed lines* are the 95% confidence levels.

the values of the correlation coefficient arrive at local minima, and the interval between these two neighboring local minima is 126 months (10.5 years).

Based on the cross-correlation analysis, both of the QBO and the ESC signal between GSF and SN are highly positive correlation. However, this method is usually used to measure the long-term variation between different solar activity indicators, causing an averaging of the property being measured, as pointed out by Deng et al. (2013c). To compare the timescales of the two data series on a point-by-point basis, another useful tool, the so-called CRP approach can be used. In our analysis, we also apply this powerful technique to reveal their phase relationship for the ESC signal.

The most important advantage of the CRP approach is that the local dependency described by bowed lines of two data sets can be determined and estimated. To construct the CRP pattern between GSF and SN for the ESC signal, the embedding dimension of three, which was calculated by many authors, is used. Fox example, Letellier et al. (2006) studied the dynamical behavior of sunspot activity by the nonlinear theory, and found that an embedding dimension equal to three is sufficient to reveal its dynamic structure. To investigate the nonlinear dynamical behavior of the polar faculae and sunspot activity for the time interval from 1951 August to 1998 December, Deng et al. (2016a) used several nonlinear time series analysis approaches, and found that both the high- and the low-latitude solar activity are governed by a three-dimensional chaotic attractor. Another important parameter for constructing the CRP pattern is the time delay, which was estimated to be varying from 29 to 31 when different indicators used (Deng et al. 2016a). Here, this value of 30 is used in our analysis. The left panel of Figure 6 displays the CRP pattern between GSF and SN for the ESC signal, with the green dashed line and the red solid line showing the main diagonal and

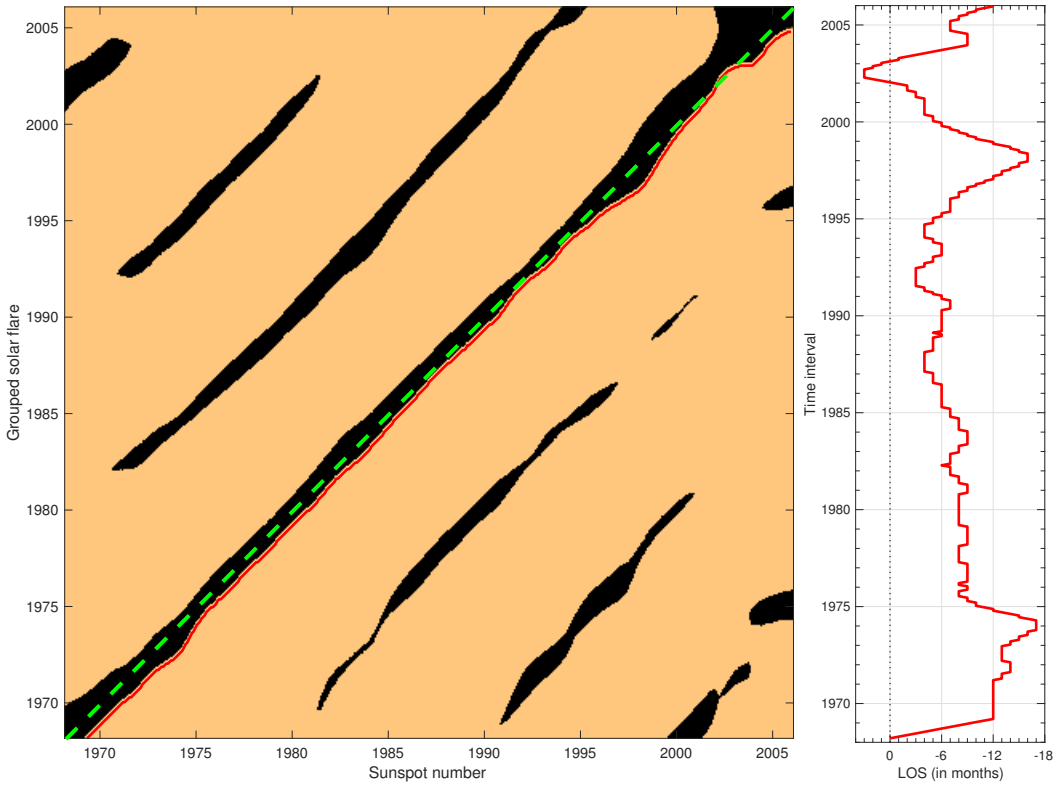

Fig. 6 *Left panel*: the CRP pattern between GSF and SN for the ESC signal, the *green dashed line* and the *red solid line* are the main diagonal and the LOS, respectively. *Right panel*: the LOS, which is used to reveal the local phase difference, extracted from the CRP pattern.

the LOS, respectively. Here the LOS could be applied to recognize which time series leads or lags in phase. From this panel, one can easily see that the LOS lies close to the main diagonal, but it still has some deflection from the main diagonal at many data points. We extracted the LOS from the CRP pattern, and showed it in the right panel of Figure 6. If the LOS is greater (smaller) than zero, the GSF will lead (lag) the SN in phase. We found that most of the LOS values are smaller than zero, and the average of all LOS values is –7.8 months. That is, the ESC signal of GSF lags in phase with 7.8 months during the considered time interval. Our analysis result is agreement and further enhances the results obtained by previous studies.

For the QBO signal, we also studied their phase relationship by the CRP technique, but no such regularity is found. Therefore, we can arrive at a conclusion that the systematic phase delays between GSF and SN originate from the inter-solar-cycle signal (the so-called ESC signal).

4 DISCUSSION

With the data sets of GSF and SN for the time interval from January 1965 to March 2009, their periodic variation and phase relationship were studied by two nonlinear time-frequency analysis techniques. First, the time series of GSF and SN were decomposed into eight IMFs and a trend through EEMD technique. Second, the significant periodicities of the first seven IMFs were studied by the significance test method. Finally, the CRP approach is applied to reveal their phase relationship at different timescales.

Based on the EEMD analysis, the extracted IMFs of both GSF and SN have time-dependent amplitudes and differ from pure sinusoidal functions. Furthermore, the significant periodicities of both GSF and SN, those are above the 99% confidence level, are connected with the differential rotation periodicity, the QBO signal, and the ESC signal. However, the specific values of these periodicities are not absolutely identical. From the CRP analysis, it is found that the ESC signal of GSF lags behind (the LOS values smaller than zero) that of SN with an average value of 7.8 months during the considered time interval, but for the QBO signal, no such systematic regularity was found. That leads us to conclude that the systematic phase delays between GSF and SN originate from the ESC signal.

There is no doubt that both GSF and SN have similar quasi-periodic features, because they have intrinsic link with the solar magnetic field. However, they are related in various ways to different aspects of magnetic processes taking place on the Sun (one is in the photosphere, and

the other one is in the corona), so their long-term variations differ in fine details. Sammis et al. (2000) studied the relationship between sunspots and large flares, and found that there is a general trend for large regions to produce large flares, but it is less significant than the dependence on magnetic class. Eren et al. (2017) analyzed different types (C, M, and X classes) of X-ray solar flares occurring in sunspot groups (a total of 4262 active regions) for the time period 1996–2014, and found that large and complex sunspot groups have the flare-production potential about eight times higher than the small and simple active regions. To understand the periodic variations and distributions of solar flares with the sunspot group numbers between 1996 July and 2016 December, Oloketuyi et al. (2019) studied the periodicities and distributions of the solar soft X-ray flares with B, C, M, and X-class. They found that the difference in periodic variations of the flare classes could be attributed to the magnetic flux system of sunspot groups producing them. Kilcik et al. (2011) analyzed the solar activity cycle by focusing on time variations of the number of sunspot groups as a function of their modified Zurich class, and found that large sunspot groups appear to reach their maximum in the middle of the solar cycle (phases 0.45–0.5), while the international sunspot numbers and the small sunspot groups generally peak much earlier (phases 0.29–0.35). We infer that this is also a possible reason for explaining the phase different (tens of months) between flare activity and sunspot activity, which has been confirmed by Deng et al. (2013b) who studied the relative phase analyses of 10.7 cm solar radio flux with sunspot numbers.

In conclusion, in this paper we showed that GSF is delayed with regard to SN with an average of 7.8 months for the period 1965–2009. The obtained phase lag is smaller than the characteristic value (in the range between 10 and 15 months) derived by Temmer et al. (2003). To understand the phase relationship between GSF and SN at different timescales, the energy balance in the flaring solar corona should be considered. From a model of the dynamic energy balance in the corona over the solar cycle, Wheatland & Litvinenko (2001) found that the expected global coronal response time (the time for flares to remove available coronal energy) is 8.8 months. A solar flare is a sudden release of magnetic energy that was stored in the corona, and the flare rate is believed to increase with the stored energy. The available magnetic energy is expected to vary cyclically with the rate of energy supply to the corona, but with a phase delay with respect to the variation in energy supply. Therefore, our analysis result is consistent with and further enhances the numerical model proposed by Wheatland & Litvinenko (2001), and may provide evidence about the storage of magnetic energy in the corona.

Acknowledgements This research uses sunspot data obtained from the WDC-SILSO, Royal Observatory of Belgium, Brussels (*http://www.sidc.be/silso/*). This work is supported by the National Key Research and Development Program of China (2018YFA0404603), the Joint Research Fund in Astronomy (Nos. U1831204, U1931141 and U1631129) under cooperative agreement between the National Natural Science Foundation of China (NSFC) and the Chinese Academy of Sciences (CAS), the NSFC (11903009), the Yunnan Key Research and Development Program (2018IA054), the open research program of the CAS Key Laboratory of Solar Activity (KLSA201807), and the major scientific research project of Guangdong regular institutions of higher learning (2017KZDXM062).

References

Aschwanden, M. J. 1994, Sol. Phys., 152, 53
Bazilevskaya, G., Broomhall, A.-M., Elsworth, Y., & Nakariakov, V. M. 2014, Space Sci. Rev., 186, 359
Cameron, R. H., Dikpati, M., & Brandenburg, A. 2017, Space Sci. Rev., 210, 367
Clette, F., Svalgaard, L., Vaquero, J. M., & Cliver, E. W. 2014, Space Sci. Rev., 186, 35
Deng, L. H., Gai, N., Tang, Y. K., Xu, C. L., & Huang, W. J. 2013a, Ap&SS, 343, 27
Deng, L. H., Li, B., Xiang, Y. Y., & Dun, G. T. 2014, Advances in Space Research, 54, 125
Deng, L. H., Li, B., Xiang, Y. Y., & Dun, G. T. 2015, Journal of Atmospheric and Solar-Terrestrial Physics, 122, 18
Deng, L. H., Li, B., Xiang, Y. Y., & Dun, G. T. 2016a, AJ, 151, 2
Deng, L. H., Li, B., Zheng, Y. F., & Cheng, X. M. 2013b, New Astron., 23, 1
Deng, L. H., Qu, Z. Q., Wang, K. R., & Li, X. B. 2012, Advances in Space Research, 50, 1425
Deng, L.-H., Qu, Z.-Q., Yan, X.-L., & Wang, K.-R. 2013c, RAA (Research in Astronomy and Astrophysics), 13, 104
Deng, L. H., Xiang, Y. Y., Qu, Z. N., & An, J. M. 2016b, AJ, 151, 70
Deng, L., Zhang, X., An, J., & Cai, Y. 2017, Journal of Space Weather and Space Climate, 7, A34
Du, Z. L. 2011, Annales Geophysicae, 29, 1005
Du, Z.-L., & Wang, H.-N. 2012, RAA (Research in Astronomy and Astrophysics), 12, 400
Eckmann, J.-P., Oliffson Kamphorst, S., & Ruelle, D. 1987, EPL (Europhysics Letters), 4, 973
Eren, S., Kilcik, A., Atay, T., et al. 2017, MNRAS, 465, 68
Feng, S., Yu, L., & Yang, Y. 2013, Bulletin of the Astronomical Society of India, 41, 237
Gao, P. X. 2017, MNRAS, 472, 2913
Gao, P.-X., Li, K.-J., & Li, F.-Y. 2017, Sol. Phys., 292, 124

Gupta, M., Mishra, V. K., & Mishra, A. P. 2007, Journal of Geophysical Research (Space Physics), 112, A05105
Huang, N. E., Shen, Z., Long, S. R., et al. 1998, Proceedings of the Royal Society of London Series A, 454, 903
Kilcik, A., Özgüç, A., Rozelot, J. P., & Ataç, T. 2010, Sol. Phys., 264, 255
Kilcik, A., Yurchyshyn, V. B., Abramenko, V., et al. 2011, ApJ, 731, 30
Letellier, C., Aguirre, L. A., Maquet, J., & Gilmore, R. 2006, A&A, 449, 379
Li, K. J., Feng, W., Xu, J. C., et al. 2012a, ApJ, 747, 135
Li, K. J., Shi, X. J., Feng, W., et al. 2012b, MNRAS, 423, 3584
Marwan, N., Carmen Romano, M., Thiel, M., & Kurths, J. 2007, Phys. Rep., 438, 237
Marwan, N., Donges, J. F., Zou, Y., Donner, R. V., & Kurths, J. 2009, Physics Letters A, 373, 4246
Marwan, N., & Kurths, J. 2002, Physics Letters A, 302, 299
Oloketuyi, J., Liu, Y., & Zhao, M. 2019, ApJ, 874, 20
Qu, Z.-N., Feng, W., & Liang, H.-F. 2015, RAA (Research in Astronomy and Astrophysics), 15, 879
Sammis, I., Tang, F., & Zirin, H. 2000, ApJ, 540, 583
Temmer, M., Veronig, A., & Hanslmeier, A. 2003, Sol. Phys., 215, 111
Wagner, W. J. 1988, Advances in Space Research, 8, 67
Wheatland, M. S., & Litvinenko, Y. E. 2001, ApJ, 557, 332
Wilson, R. M. 1993, J. Geophys. Res., 98, 11
Wu, Z., & Huang, N. E. 2004, Proceedings of the Royal Society of London Series A, 460, 1597
Wu, Z., & Huang, N. E. 2011, Advances in Adaptive Data Analysis, 1, 1
Xiang, N. B., & Qu, Z. N. 2016, AJ, 151, 76
Xiang, N. B., Qu, Z. N., & Zhai, Q. 2014, AJ, 148, 12
Zbilut, J. P., Giuliani, A., & Webber, Jr., C. L. 1998, Physics Letters A, 246, 122